



Cite this: *Sustainable Energy Fuels*, 2023, 7, 812

Received 29th September 2022
Accepted 20th December 2022

DOI: 10.1039/d2se01350a

rs.c.li/sustainable-energy

High-throughput identification of materials for silicon tandem solar cells†

Yanzhen Zhao,^a Zhikun Yao,^a Chang Liu,^{id}^a Wei Ren,^{id}^{ab} Geoffroy Hautier^c and Lee A. Burton^{id}^{*ad}

High-throughput *ab initio* calculations are employed to identify the most promising materials for Si tandem solar cells. Starting with the Materials Project database of more than 131 000 materials, we evaluate the relevant properties of thermodynamic stability, lattice mismatch with silicon, band gap, effective mass, optical absorption coefficient and dynamic stability. The identified 11 optimal candidates represent a variety of material chemistries with oxides, pnictogenides, and chalcogenides included. Among them, perhaps the most promising is $\text{Cu}_2\text{ZnSiSe}_4$, which has almost ideal properties for all physical criteria and is composed of relatively earth-abundant constituents.

Introduction

Energy generation accounts for about 70 percent of total greenhouse gas emissions,¹ which are driving an unsustainable shift in the earth's climate.² Therefore, it is urgent that renewable energy technologies be deployed as much as possible to offset emissions and reduce the extent of the greenhouse effect.

The potential for renewable energy is enormous because it can in principle exceed the world's energy demand many thousand times over.³ Among renewable sources, the largest reservoir of potential energy is from sunlight or solar energy. Photovoltaic (PV) cells directly convert sunlight into electricity, offering a practical and sustainable solution to the challenge of cleanly meeting global energy demand.⁴

Today, more than 90% of the market share of PV uses silicon (Si) as an absorber material.⁵ However, it is well established that Si is not an optimal light absorber as it has a band gap that is both indirect and lower than ideal according to the Shockley–Queisser efficiency limit.⁶ While some researchers seek alternate technologies to supplant silicon solar cells, building on the existing success of Si is the most efficient way to increase PV deployment.⁷ Therefore, a dual-junction device is desirable, which uses two materials to absorb different portions of the solar spectrum in the same cell rather than one. As shown in Fig. 1, by moving from a single to double junction, the low band

gap of Si can be complemented with a high band gap material that together would capture a much larger fraction of the solar spectrum.^{4,8} The indirect gap of Si is also ameliorated as non-radiative recombination becomes less important with the decrease in internal carrier concentrations.⁹

Fortunately, the properties needed for an ideal Si junction partner are already known, assuming a 2-terminal device configuration. These properties are thermodynamic and dynamic stability, lattice match with silicon, a band gap of 1.74 eV, low charge effective masses and high optical absorption coefficient. (Lattice matching with silicon can be neglected for 4-terminal tandem devices but they require more components that then have their own stringent property requirements. Each additional device component leads to higher cost and introduces possible sources of efficiency loss and so 4-terminal cells are not considered further in this work). Knowing the desirable physical properties allows for an effective high-throughput (HT) search of known materials to be performed. Over the past

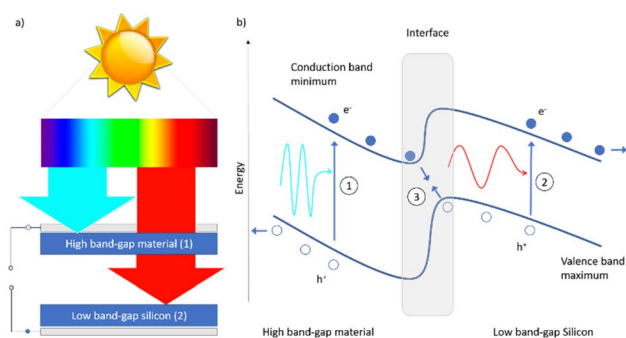


Fig. 1 (a) Schematic of dual-junction material device and (b) the energetic principles of operation. (1) Higher energy absorption by the top layer, (2) lower energy absorption by Si (3) recombination at the interface. Holes and electrons are extracted at opposite contacts.

^aInternational Centre for Quantum and Molecular Structures, Department of Physics, Shanghai University, Shanghai 200444, China. E-mail: laburto@gmail.com

^bZhejiang Laboratory, Hangzhou 311100, China

^cThayer School of Engineering, Dartmouth College, Hanover, New Hampshire 03755, USA

^dDepartment of Materials Science and Engineering, The Ilby and Aladar Fleischman Faculty of Engineering, Tel Aviv University, Ramat Aviv, Tel Aviv 6997801, Israel

† Electronic supplementary information (ESI) available. See DOI: <https://doi.org/10.1039/d2se01350a>

decade, computational material screening and high throughput (HT) methods has enabled the creation of publicly available databases with calculated properties of hundreds of thousands of materials,^{10–15} from which optimal materials for specific applications can be sought. For example, HT computing has been applied to various fields such as energy storage,^{16–19} catalysis,^{20,21} or topological insulators.^{22–24} The method has also previously been applied to the field of photovoltaics,^{25–28} including perovskite–perovskite tandem cells,²⁹ although not to the junction partner of Si tandem to the authors knowledge.

In this paper, we present the *ab initio* HT screening of materials to identify those that are best able to complement crystalline silicon for a hypothetical dual junction device. Beginning with all entries of the Materials Project (over 130 thousand),¹² we evaluate the relevant properties of thermodynamic stability, lattice mismatch with silicon, band gap, effective mass and optical absorption coefficient. Ultimately, we find 11 very promising materials: LiAsS₂, WO₃, Y₂TeO₂, BeSiAs₂, Dy₂TeO₂, Tb₂Ti₂S₂O₅, Tb₂TeO₂, SrLi₄N₂, Li₂TiN₂, CuGaGeSe₄, and Cu₂ZnSiSe₄, which is perhaps the most promising of all.

Methods

The structures and properties of the Materials Project were accessed through the Python Materials Genomics (pymatgen) application programming interface (API)³⁰ and analyzed through the pymatgen open-source Python library.³¹

Density functional theory (DFT)³² calculations were performed using the Vienna *Ab initio* Simulation Package (VASP).³³ Projector augmented wave (PAW) pseudopotentials with a cutoff of 500 eV were used.^{34,35} For structural optimization the Perdew–Burke–Ernzerhof (PBE)³⁶ form of the generalized gradient approximation (GGA) was used.³⁷ Brillouin zone integration was performed on a Monkhorst–Pack *k*-point mesh.³⁸ All VASP input files were automatically generated by pymatgen “io.vasp.sets” module. All computations are performed with spin polarization and with magnetic ions in a high-spin ferromagnetic configuration initially, allowing the system to relax to a low spin state during over the course of the calculation.

The convex hull of computed total energies is used to evaluate stability. To improve upon PBE band gaps, we used the Heyd–Scuseria–Ernzerhof (HSE) screened hybrid exchange–correlation functional,³⁹ with a shielding distance of 0.207 Å^{−1} and 25% Hartree–Fock exchange. Effective masses are calculated by the Boltzmann Transport Properties (BoltzTrap2)⁴⁰ software interfaced within pymatgen. BoltzTraP is a semi-classical method based on smoothed Fourier interpolation of the bands, which utilizes a temperature-independent and isotropic constant relaxation time approximation.⁴¹ Absorption coefficient is calculated by using the independent particle approximation (IPA) within DFT to obtain the imaginary part of the dielectric constant and use mathematical properties Kramers–Kronig relations to get their real part. From these, the absorption coefficient is calculated using VASPKIT.⁴² Phonon calculations are performed by Phonopy interfaced with VASP. To obtain reasonable lattice parameters, we used the PBESol

function to optimize all structures with a 2 × 2 × 2 supercell and a 5 × 5 × 5 gamma-centred *K*-point grid for all materials.

A summary of the full screening procedure is shown in Fig. 2 and in Table 1.

Results

The data of 131 613 materials was available in the Materials Project database at the commencement of this work.¹² Beginning with all of them, we first screen out any material that could be considered intrinsically unstable. We do this by eliminating any material with an energy above convex hull (E_{hull}) of more than 0 eV per atom. E_{hull} is the energy released by decomposition of a compound into other materials of the same components and an E_{hull} of 0 eV per atom means no such processes are favourable.⁴³ These results are provided at the PBE level of theory, which is known to agree well with experiment.⁴⁴ Other HT studies allow for a margin of error with this term of the order of $\pm K_{\text{B}}T$,^{27,45} but enforcing this screening criterion of $E_{\text{hull}} = 0$ eV still provides a large number of possible candidates of 33 145 here.

Beyond component stability, the successful operation of a Si dual junction cell requires an efficient charge transport interface between the top layer and Si. If both materials have commensurate lattices it will be easier to form a junction. In fact, if the components match well enough, it may be possible to forgo a buffer layer entirely as it is often the purpose of a buffer layer to facilitate lattice mismatch.⁴⁶ The consideration of lattice match with Si has even been reported to play a more significant role in device performance than band gap matching.⁴⁷ We use the pymatgen’s ‘Symmetry Analyzer module’ to convert primitive cells to conventional standard structure,⁴⁸ and then use the ‘Substrate Analyzer module’ to quantify lattice mismatch.⁴⁹ The class ‘Substrate Analyzer’ uses the topological search by Zur and McGill to identify matching super-lattices on various faces of the two materials,⁵⁰ and calculates a common unit cell area as the minimal coincident interface area (MCIA).

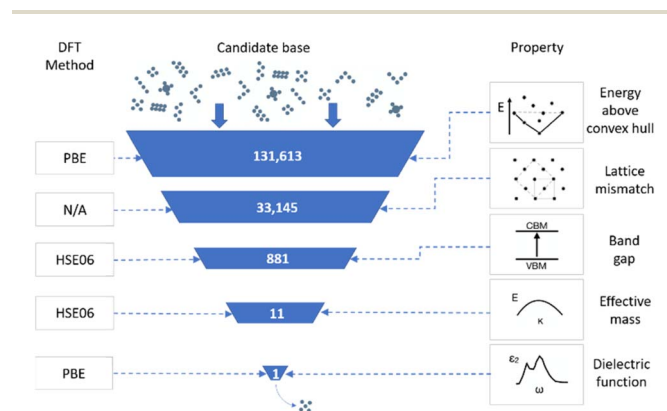


Fig. 2 An illustration of the full screening procedure. The funnel-like shape in the centre depicts the narrowing candidate pool. On the right is a representation of the property sought at each stage and on the left is the corresponding level of theory.

Table 1 The selection and screening criteria for all properties in this study

Property	Screening criteria
Thermodynamic stability	Energy above hull = 0 eV
Lattice match with Si	Minimal coincident interface area with Si of 29.9 Å ²
Band gap	Between 1.64–1.84 eV
Dynamic stability	Weak imaginary phonon modes
Effective mass	The smallest possible values for electrons
Optical absorption coefficient	Most rapid absorption coefficient onset

To illustrate the effectiveness of MCIA we show two values for materials matched with silicon in Fig. 3. Vanadium boride is selected as an example material with a very high MCIA and cerium dioxide as an example with the minimum MCIA with Si, which are 358.9 Å² and 29.9 Å² respectively. It can be seen that CeO₂ and Si have similar lattice parameters and atom-to-atom distances within the structure. However, the lattice parameters and the distance between the atoms in the structure of VB and Si differ greatly. As a result, a smaller value of MCIA can be considered to correspond to a higher degree of lattice match with Si. Selecting only the materials with the smallest obtained MCIA with Si to proceed in the screening reduces the number of candidate materials from 33 145 to 881.

For the third screening stage, materials with band gaps close to ideal for a Si tandem partner are sought. The optimum band gap value has been reported to be around 1.74 eV in earlier work,^{51–53} thus we seek materials with band gaps between 1.64 and 1.84 eV *i.e.* ± 0.1 eV of the ideal target. To this end, we analyse the 881 materials to survive the screening steps so far at the HSE06 level of theory. This computational method is known to obtain more reliable band gaps than DFT,^{54,55} which we confirm for silicon itself: Si has a band gap of 0.853 eV at the PBE level, 1.20 eV at HSE06 and 1.23 eV in experiment.⁵⁶ HSE06 has also proven to be capable of giving close-to- experiment predictions for a large range of compounds in other high-throughput screening studies.²⁵

The full list of 881 chemical formulae and corresponding HSE band gaps are provided in the ESI (Table S1†), arranged in ascending order of gap value. More than half of these materials

are metallic, which would be unsuitable for any photovoltaic application but the selection window of 1.64 and 1.84 eV includes the following 11 materials: LiAsS₂,⁵⁷ WO₃,⁵⁸ CuGaGeSe₄,⁵⁹ Y₂TeO₂, Cu₂ZnSiSe₄,⁶⁰ BeSiAs₂,⁶¹ Dy₂TeO₂,⁶² Tb₂-Ti₂S₂O₅,⁶³ Tb₂TeO₂,⁶² SrLi₄N₂ (ref. 64) and Li₂TiN₂. The HSE06 band gaps for these materials are shown in Fig. 4 and the chemical structures of all 11 materials are shown in ESI Fig. S1.†

Note that some of the candidates have no providence or citation for original synthesis in the Materials Project. The compounds for which we find no experimental report (to wit Y₂TeO₂ and Li₂TiN₂) were likely added to the Materials Project database by structure prediction methods, but are still on the convex hull with respect to competing phases. This observation prompted us to investigate the dynamic stability by calculating phonons for each material, especially considering that even structures on the convex hull can be dynamically unstable.⁶⁵ The phonon band structures for each of the eleven candidates are included in the ESI (Fig. S2†). While dynamic stability can be instructive for bulk materials, it may be less important in a tandem device application that we consider here due to the epitaxial strain provided by the Si substrate. Furthermore, many structures, including well-studied perovskites, predicted to be dynamically unstable from phonon calculations are actually stable at finite temperatures.⁶⁵ Regardless, the phonons show a surprising degree of instability for some of the candidates. Li₂TiN₂, LiAsS₂, Y₂TeO₂ and WO₃ each show strong negative frequency *i.e.* imaginary modes that could preclude their isolation in experiment. Of these, LiAsS₂ has been considered for thermoelectric,⁶⁶ and photovoltaic applications previously,^{57,67} while Li₂TiN₂ and Y₂TeO₂ have little to no precedent

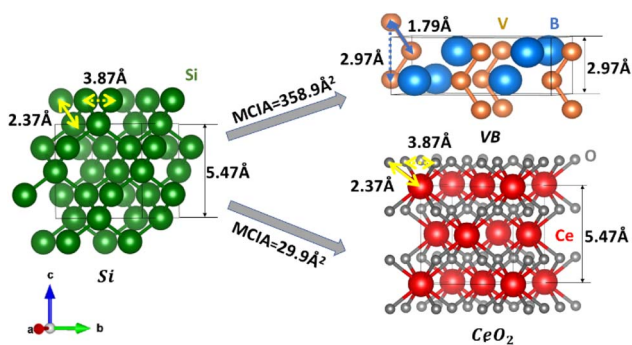


Fig. 3 The calculated minimal coincident interface area (MCIA) of Si with CeO₂ (358.9 Å²) and VB (29.9 Å²). It can be seen that the lower MCIA value provides a much closer lattice match to Si. Si atoms are in green, V in orange, B in blue, Ce in red and O in grey.

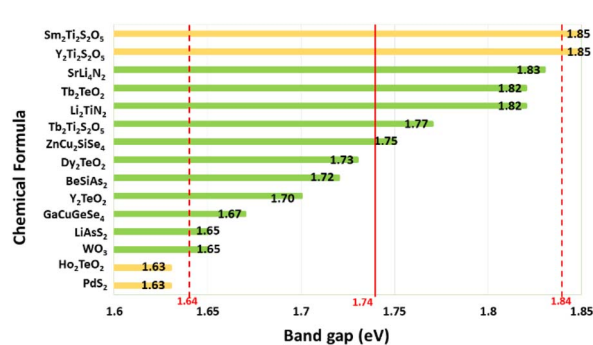


Fig. 4 The 11 candidate materials (in green) identified by range of ±0.1 eV around the optimum gap value of an Si junction partner (red). Also shown (in yellow) are the materials just outside of either end of the selection window.

in the experimental literature. WO_3 has been explored for photo-electrochemical water splitting,⁶⁸ and electrochromic window applications previously.⁶⁹ However, it is noted that the literature surrounding this material is “somewhat confusing”,⁷⁰ most probably due to the fact that there are at least 4 different WO_3 structures each of which has distinct electronic properties. For this screening work we identify the so called tetragonal phase with $P4/nmm$ [129] symmetry but there is also a $P4/ncc$ [130] structure, a $Pbcn$ [60] structure and a $Pbcm$ [57] structure denoted to be on the convex hull by the Materials Project, with several others within $K_B T$ of the hull. However, a more detailed study finds that the 4 stable structures are not equivalent and the structure identified by our screening is not on the convex hull or dynamically stable (in agreement with our phonon analysis).⁷¹ Rather than omit this WO_3 , we include it for transparency and to serve as a cautionary reminder about the inherent pitfalls of any high-throughput study.

Returning to the electron properties, we calculate the band structure diagrams for the 11 candidates as shown in the ESI (Fig. S3†). Equipped with the more reliable HSE06 electronic structure, it is possible to further explore candidate's suitability. Efficient transport of the generated charge carriers after light absorption is required for low losses in PV materials.¹⁰ Effective mass is used to describe the transport capabilities of a material,⁷² with charge mobility inversely proportional to the effective mass.⁷³ Highly mobile charges are more likely to be able to reach the device electrodes before recombining, significantly improving device performance.

Charge effective mass is an intrinsic materials property related to the dispersion of the bands around the Fermi level. In order to take into account the full range of bands for each material, the effective mass values were calculated by the linearized Boltzmann transport equation.⁴⁰ In this work we use BoltzTraP with the constant relaxation time approximation.⁷⁴

The conductivity effective mass tensor is dependent on the values of temperature and doping concentration. We assume a dopant concentration of 10^{16} cm^{-3} and a temperature of 300 K. From this, the average effective mass can be derived from relevant pockets in the Brillouin zone around the Fermi level.⁷⁵

Table 2 The predicted charge effective mass for holes (m_p^*) and electrons (m_n^*) with a HSE electronic structure, a doping concentration of 10^{16} cm^{-3} and temperature of 300 K. The table is sorted in order of electron effective mass from smallest to largest

MP-id	Material	HSE m_p^*	HSE m_n^*
1232332	$\text{Cu}_2\text{ZnSiSe}_4$	0.93, 1.20, 1.20	0.16, 0.17, 0.17
15845	SrLi_4N_2	2.34, 2.34, 126.38	0.28, 0.35, 0.35
1009087	BeSiAs_2	0.42, 0.64, 0.64	0.39, 0.39, 0.46
1224851	CuGaGeSe_4	0.39, 0.39, 2.47	0.70, 0.70, 2.14
1245502	Li_2TiN_2	0.34, 0.34, 3.52	0.65, 0.65, 2.22
19443	WO_3	1.09, 1.09, 2.33	1.07, 1.07, 2.80
555874	LiAsS_2	0.52, 0.71, 1.17	0.16, 0.51, 6.65
755756	Y_2TeO_2	0.27, 0.27, 10.74	0.81, 0.81, 45.22
16036	Tb_2TeO_2	0.29, 0.29, 12.11	1.05, 1.05, 89.38
16037	Dy_2TeO_2	0.28, 0.28, 7.02	0.93, 0.93, 98.47
10960	$\text{Tb}_2\text{Ti}_2\text{S}_2\text{O}_5$	0.55, 0.55, 212.31	0.58, 0.58, 527.53

Because silicon can be extrinsically doped p- or n-type,⁷⁶ in Table 2 we list both the effective mass of p-type doping and n-type doping for each candidate material.

The atomic structure configurations of the candidates (see Fig. S1†) are reflected in the effective mass tensors. For example, the materials Dy_2TeO_2 , Y_2TeO_2 , Tb_2TeO_2 have identical structures with $I4/mmm$ symmetries (number 139) and have very similar effective mass tensors. Similarly, the structure of $\text{Tb}_2\text{-Ti}_2\text{S}_2\text{O}_5$ appears highly anisotropic, as is the corresponding effective mass. Ultimately, the smallest possible values of charge effective mass are sought in as many directions as possible. In this regard, $\text{Cu}_2\text{ZnSiSe}_4$, CuGaGeSe_4 and BeSiAs_2 are among the most ideal, with LiAsS_2 , Li_2TiN_2 and WO_3 somewhat behind. SrLi_4N_2 has favourable electron mass properties but relatively unfavourable hole effective mass. Dy_2TeO_2 , Y_2TeO_2 , Tb_2TeO_2 , and $\text{Tb}_2\text{Ti}_2\text{S}_2\text{O}_5$ are perhaps the least suitable with very high masses in at least one direction.

The final stage of analysis pertains to light absorption as indicated by absorption coefficient as a function of photon energy. The higher the absorption coefficient for any given energy, the shorter the distance that light penetrates into the material before being absorbed.⁷⁷ A stronger absorption coefficient therefore allows for a thinner absorber layer, which reduces both material and processing costs for a PV device.⁷⁸

The frequency dependent dielectric matrix is calculated from the ground state electron configuration at the PBE level of theory and used to calculate absorption coefficient. The absorption profiles are then individually shifted to match the more accurate HSE06 band gaps for light absorption onset for that material, which has been shown to be an effective approach previously.⁷⁹ Each of the plots of absorption coefficient for the 11 candidate materials is shown in the ESI, Fig. S4.† Fig. 5 shows all of these individual absorption profiles superimposed together.

The ideal Si junction partner would display as rapid an onset of absorption as possible to allow for a thinner absorber layer. Thinness of absorber layer is one of the most effective ways to

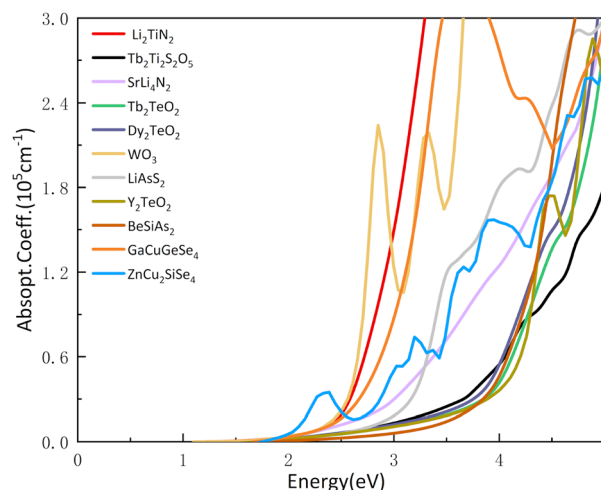


Fig. 5 Superposition of the light absorption coefficients calculated for the 11 final-candidate material as a function of energy.

Table 3 The results of the full screening procedure summarised for every final candidate

Material	Energy above convex hull	Si minimal coincident interface area	Imaginary phonons?	Band gap	Hole effective mass	Electron effective mass
ZnCu ₂ SiSe ₄	0 eV	29.9 Å ²	No	1.75 eV	0.93, 1.20, 1.20	0.16, 0.17, 0.17
BeSiAs ₂	0 eV	29.9 Å ²	No	1.72 eV	0.42, 0.64, 0.64	0.39, 0.39, 0.46
GaCuGeSe ₄	0 eV	29.9 Å ²	No	1.67 eV	0.39, 0.39, 2.47	0.70, 0.70, 2.14
SrLi ₄ N ₂	0 eV	29.9 Å ²	No	1.83 eV	2.34, 2.34, 126.38	0.28, 0.35, 0.35
Li ₂ TiN ₂	0 eV	29.9 Å ²	Yes	1.82 eV	0.34, 0.34, 3.52	0.65, 0.65, 2.22
WO ₃	0 eV	29.9 Å ²	Yes	1.65 eV	1.09, 1.09, 2.33	1.07, 1.07, 2.80
LiAsS ₂	0 eV	29.9 Å ²	Yes	1.65 eV	0.52, 0.71, 1.17	0.16, 0.51, 6.65
Y ₂ TeO ₂	0 eV	29.9 Å ²	Yes	1.70 eV	0.27, 0.27, 10.74	0.81, 0.81, 45.22
Tb ₂ TeO ₂	0 eV	29.9 Å ²	Yes	1.82 eV	0.29, 0.29, 12.11	1.05, 1.05, 89.38
Dy ₂ TeO ₂	0 eV	29.9 Å ²	Yes	1.73 eV	0.28, 0.28, 7.02	0.93, 0.93, 98.47
Tb ₂ Ti ₂ S ₂ O ₅	0 eV	29.9 Å ²	No	1.77 eV	0.55, 0.55, 212.31	0.58, 0.58, 527.53

minimise costs,^{80,81} thereby allowing the device to be more cost effective when compared to other methods of energy generation.⁸² For the candidates we identify, it's possible to see quite a varied response in their light absorption profiles. The least well performing light absorbers appear to be Tb₂Ti₂S₂O₅, Tb₂TeO₂, BeSiAs₂ and Dy₂TeO₂ with steep onsets that don't occur until around 4 eV (310 nm photon wavelength). On the other hand, the best 3 performing materials appear to be Cu₂ZnSiSe₄, WO₃ and Li₂TiN₂. Cu₂ZnSiSe₄ has a more rapid initial onset than the other candidates but this initial advantage is lost at higher energies of light where WO₃ becomes more highly absorbing. Finally, at around 3 eV, Li₂TiN₂ becomes the strongest light absorber-although this is already beyond the visible light spectrum.

Considering both charge effective mass and absorption coefficient, it can be seen that Cu₂ZnSiSe₄ performs most favourably for both, with WO₃ and Li₂TiN₂ in close competition as well. However, WO₃ and Li₂TiN₂ were 2 of the materials found to have quite strong dynamic instability, whereas Cu₂ZnSiSe₄ was highly stable. What's more, Cu₂ZnSiSe₄ has a band gap that is joint-closest to the ideal value and is composed of relatively abundant constituent elements.

The material Cu₂ZnSiSe₄ is perhaps the most exciting candidate of all compounds considered in this study, not just because of its intrinsically favourable properties but also because of its likely tuneable nature provided by the large composition variability. The compounds Cu₂ZnSiSe₄ and CuGaGeSe₄ (which also performs well in our screening by properties) are closely related to each other chemically and to the well-studied material Cu₂ZnSnSe₄ (CZTSe), these are called kesterite chalcogenides, being typically 4-component systems with the $\bar{I}4$ [82] symmetry in the ground state.⁸³ Kesterite materials are well known for cation miscibility allowing for the careful tuning of physical properties by varying the chemical compositions within the same structure.⁸⁴ CZTSe also has a record PV device efficiency of 12.6% as a single junction absorber material,⁸⁵ further suggesting that Cu₂ZnSiSe₄ and CuGaGeSe₄ could perform well in photovoltaic applications.

To the knowledge of the authors no tandem device of Si with Cu₂ZnSiSe₄ has been reported before, although it was suggested as an ideal candidate for this application elsewhere in the

recent literature,⁸⁶ thereby effectively validating our high-throughput approach. There is an orthorhombic Cu₂ZnSiSe₄ that has been previously identified in experiment,⁸⁷ and confirmed in single crystals down to 150 K,⁸⁸ but it is found to be higher on the convex hull than the tetragonal $\bar{I}4$ material that our screening identifies. DFT has shown to be a powerful tool in structure prediction and materials discovery,⁸⁹ and while there is an inevitable margin for error the agreement of the ground state found here and the known literature on CZTSe gives a high level of confidence in our identification of the material as a suitable candidate. Furthermore, the existing body of knowledge surrounding kesterite growth and deposition (for example chemical bath deposition,⁹⁰ electrodeposition,⁹¹ pulsed laser deposition,⁹² and slurry deposition,⁹³ to name a few) should greatly facilitate experimental exploration of these candidates.

Conclusions

In conclusion, we have identified a series of promising materials for Si tandem solar cells from all 131 613 materials in the Materials Project. We provide the HSE06 band gaps for 881 stable materials that are a lattice match with silicon. Of these, we identify 11 materials (LiAsS₂, WO₃, CuGaGeSe₄, Y₂TeO₂, Cu₂ZnSiSe₄, BeSiAs₂, Dy₂TeO₂, Tb₂Ti₂S₂O₅, Tb₂TeO₂, SrLi₄N₂, Li₂TiN₂) that have almost ideal band gaps. Among them, the materials closest to the ideal band gap are Cu₂ZnSiSe₄ and Dy₂TeO₂.

For charge transport, Cu₂ZnSiSe₄, CuGaGeSe₄ and BeSiAs₂ have the favourable charge effective masses and, Cu₂ZnSiSe₄, WO₃ and Li₂TiN₂ have the most favourable absorption profiles. Given the dynamic instabilities predicted for Li₂TiN₂, LiAsS₂, Y₂TeO₂ and WO₃ we conclude that Cu₂ZnSiSe₄ is perhaps the highest priority candidate for Si tandem photovoltaics currently. A full summary of results for each candidate is provided in Table 3.

While all of these materials are present in the Materials Project, and some work has begun on considering them for optoelectronic applications, we find ample scope for discovery as several of the candidates have yet to be synthesised and several others are expected to be chemically tuneable. There are also many avenues for future computational analysis such as

defect/dopant calculations or applying similar high-throughput screening approaches to the other necessary device components of a tandem cell. So-called slab calculations can also provide important properties such as band offsets and potential interface degradation reactions directly,⁹⁴ although there are too many possible slabs to enumerate in a high-throughput study such as this.

Conflicts of interest

There are no conflicts to declare.

Acknowledgements

L. A. B. and W. R. acknowledge support by the Shanghai Municipal Science and Technology Commission Program, 19010500500, 22XD1400900, 20501130600, 21JC1402700, 21JC1402600 and the Natural National Science Foundation of China (NSFC), 51950410585, 12074241, 11929401.

References

- 1 T. K. Mideksa and S. Kallbekken, The Impact of Climate Change on the Electricity Market: A Review, *Energy Policy*, 2010, **38**(7), 3579–3585, DOI: [10.1016/j.enpol.2010.02.035](https://doi.org/10.1016/j.enpol.2010.02.035).
- 2 IPCC – Intergovernmental Panel on Climate Change, <https://report.ipcc.ch/ar6wg2/index.html>, accessed 2022-03-07.
- 3 O. Ellabban, H. Abu-Rub and F. Blaabjerg, Renewable Energy Resources: Current Status, Future Prospects and Their Enabling Technology, *Renewable Sustainable Energy Rev.*, 2014, **39**, 748–764, DOI: [10.1016/j.rser.2014.07.113](https://doi.org/10.1016/j.rser.2014.07.113).
- 4 A. Polman, M. Knight, E. C. Garnett, B. Ehrler and W. C. Sinke, Photovoltaic Materials: Present Efficiencies and Future Challenges, *Science*, 2016, **352**(6283), aad4424, DOI: [10.1126/science.aad4424](https://doi.org/10.1126/science.aad4424).
- 5 H. S. Ullal, Thin Film CIGS and CdTe Photovoltaic Technologies: Commercialization, Critical Issues, and Applications, presented at the *22nd European Photovoltaic Solar Energy Conference (PVSEC) and Exhibition Milan Italy, NREL/CP-520-42058*, 2007, <https://www.nrel.gov/docs/fy07osti/42058.pdf>.
- 6 W. Shockley and H. J. Queisser, Detailed Balance Limit of Efficiency of p-n Junction Solar Cells, *J. Appl. Phys.*, 1961, **32**(3), 510–519, DOI: [10.1063/1.1736034](https://doi.org/10.1063/1.1736034).
- 7 M. A. Green, Commercial Progress and Challenges for Photovoltaics, *Nat. Energy*, 2016, **1**(1), 1–4, DOI: [10.1038/nenergy.2015.15](https://doi.org/10.1038/nenergy.2015.15).
- 8 J. Y. Kim, K. Lee, N. E. Coates, D. Moses, T.-Q. Nguyen, M. Dante and A. J. Heeger, Efficient Tandem Polymer Solar Cells Fabricated by All-Solution Processing, *Science*, 2007, **317**(5835), 222–225, DOI: [10.1126/science.1141711](https://doi.org/10.1126/science.1141711).
- 9 M. A. Green and S. P. Bremner, Energy Conversion Approaches and Materials for High-Efficiency Photovoltaics, *Nat. Mater.*, 2017, **16**(1), 23–34, DOI: [10.1038/nmat4676](https://doi.org/10.1038/nmat4676).
- 10 K. Kuhar, M. Pandey, K. S. Thygesen and K. W. Jacobsen, High-Throughput Computational Assessment of Previously Synthesized Semiconductors for Photovoltaic and Photoelectrochemical Devices, *ACS Energy Lett.*, 2018, **3**(2), 436–446, DOI: [10.1021/acseenergylett.7b01312](https://doi.org/10.1021/acseenergylett.7b01312).
- 11 S. Kirklin, J. E. Saal, B. Meredig, A. Thompson, J. W. Doak, M. Aykol, S. Rühl and C. Wolverton, The Open Quantum Materials Database (OQMD): Assessing the Accuracy of DFT Formation Energies, *npj Comput. Mater.*, 2015, **1**(1), 15010, DOI: [10.1038/npjcompumats.2015.10](https://doi.org/10.1038/npjcompumats.2015.10).
- 12 A. Jain, S. P. Ong, G. Hautier, W. Chen, W. D. Richards, S. Dacek, S. Cholia, D. Gunter, D. Skinner, G. Ceder and K. A. Persson, Commentary: The Materials Project: A Materials Genome Approach to Accelerating Materials Innovation, *APL Mater.*, 2013, **1**(1), 011002, DOI: [10.1063/1.4812323](https://doi.org/10.1063/1.4812323).
- 13 S. Curtarolo, W. Setyawan, G. L. W. Hart, M. Jahnatek, R. V. Chepulskii, R. H. Taylor, S. Wang, J. Xue, K. Yang, O. Levy, M. J. Mehl, H. T. Stokes, D. O. Demchenko and D. Morgan, AFLOW: An Automatic Framework for High-Throughput Materials Discovery, *Comput. Mater. Sci.*, 2012, **58**, 218–226, DOI: [10.1016/j.commatsci.2012.02.005](https://doi.org/10.1016/j.commatsci.2012.02.005).
- 14 L. M. Ghiringhelli, C. Carbogno, S. Levchenko, F. Mohamed, G. Huhs, M. Lüders, M. Oliveira and M. Scheffler, Towards Efficient Data Exchange and Sharing for Big-Data Driven Materials Science: Metadata and Data Formats, *npj Comput. Mater.*, 2017, **3**(1), 1–9, DOI: [10.1038/s41524-017-0048-5](https://doi.org/10.1038/s41524-017-0048-5).
- 15 *Database Creation, Visualization, and Statistical Learning for Polymer Li+-Electrolyte Design | Chemistry of Materials*, <https://pubs.acs.org/doi/abs/10.1021/acs.chemmater.0c04767>, accessed 2022-06-06.
- 16 G. Ceder, G. Hautier, A. Jain and S. P. Ong, Recharging Lithium Battery Research with First-Principles Methods, *MRS Bull.*, 2011, **36**(3), 185–191, DOI: [10.1557/mrs.2011.31](https://doi.org/10.1557/mrs.2011.31).
- 17 G. Hautier, A. Jain, S. P. Ong, B. Kang, C. Moore, R. Doe and G. Ceder, Phosphates as Lithium-Ion Battery Cathodes: An Evaluation Based on High-Throughput *Ab Initio* Calculations, *Chem. Mater.*, 2011, **23**(15), 3495–3508, DOI: [10.1021/cm200949v](https://doi.org/10.1021/cm200949v).
- 18 G. Hautier, A. Jain, H. Chen, C. Moore, S. P. Ong and G. Ceder, Novel Mixed Polyanions Lithium-Ion Battery Cathode Materials Predicted by High-Throughput *Ab Initio* Computations, *J. Mater. Chem.*, 2011, **21**(43), 17147, DOI: [10.1039/c1jm2216a](https://doi.org/10.1039/c1jm2216a).
- 19 T. Mueller, G. Hautier, A. Jain and G. Ceder, Evaluation of Tavorite-Structured Cathode Materials for Lithium-Ion Batteries Using High-Throughput Computing, *Chem. Mater.*, 2011, **23**(17), 3854–3862, DOI: [10.1021/cm200753g](https://doi.org/10.1021/cm200753g).
- 20 L. A. Burton, F. Ricci, W. Chen, G.-M. Rignanese and G. Hautier, High-Throughput Identification of Electrides from All Known Inorganic Materials, *Chem. Mater.*, 2018, **30**(21), 7521–7526, DOI: [10.1021/acs.chemmater.8b02526](https://doi.org/10.1021/acs.chemmater.8b02526).
- 21 W. F. Maier, K. Stöwe and S. Sieg, Combinatorial and High-Throughput Materials Science, *Angew. Chem., Int. Ed.*, 2007, **46**(32), 6016–6067, DOI: [10.1002/anie.200603675](https://doi.org/10.1002/anie.200603675).
- 22 H. Lin, L. A. Wray, Y. Xia, S. Xu, S. Jia, R. J. Cava, A. Bansil and M. Z. Hasan, Half-Heusler Ternary Compounds as New Multifunctional Experimental Platforms for

- Topological Quantum Phenomena, *Nat. Mater.*, 2010, **9**(7), 546–549, DOI: [10.1038/nmat2771](https://doi.org/10.1038/nmat2771).
- 23 S. Chadov, X. Qi, J. Kübler, G. H. Fecher, C. Felser and S. C. Zhang, Tunable Multifunctional Topological Insulators in Ternary Heusler Compounds, *Nat. Mater.*, 2010, **9**(7), 541–545, DOI: [10.1038/nmat2770](https://doi.org/10.1038/nmat2770).
- 24 S. Curtarolo, G. L. W. Hart, M. B. Nardelli, N. Mingo, S. Sanvito and O. Levy, The High-Throughput Highway to Computational Materials Design, *Nat. Mater.*, 2013, **12**(3), 191–201, DOI: [10.1038/nmat3568](https://doi.org/10.1038/nmat3568).
- 25 N. Sarmadian, R. Saniz, B. Partoens, D. Lamoen, K. Volety, G. Huyberegts and J. Paul, High Throughput First-Principles Calculations of Bixbyite Oxides for TCO Applications, *Phys. Chem. Chem. Phys.*, 2014, **16**(33), 17724–17733, DOI: [10.1039/C4CP02788D](https://doi.org/10.1039/C4CP02788D).
- 26 D. H. Fabini, M. Koerner and R. Seshadri, Candidate Inorganic Photovoltaic Materials from Electronic Structure-Based Optical Absorption and Charge Transport Proxies, *Chem. Mater.*, 2019, **31**(5), 1561–1574, DOI: [10.1021/acs.chemmater.8b04542](https://doi.org/10.1021/acs.chemmater.8b04542).
- 27 D. Dahlliah, G. Brunin, J. George, V.-A. Ha, G.-M. Rignanese and G. Hautier, High-Throughput Computational Search for High Carrier Lifetime, Defect-Tolerant Solar Absorbers, *Energy Environ. Sci.*, 2021, **14**(9), 5057–5073, DOI: [10.1039/D1EE00801C](https://doi.org/10.1039/D1EE00801C).
- 28 Z. Huo, S.-H. Wei and W.-J. Yin, High-Throughput Screening of Chalcogenide Single Perovskites by First-Principles Calculations for Photovoltaics, *J. Phys. D: Appl. Phys.*, 2018, **51**(47), 474003, DOI: [10.1088/1361-6463/aae1ee](https://doi.org/10.1088/1361-6463/aae1ee).
- 29 *Computational high throughput screening of inorganic cation based halide perovskites for perovskite only tandem solar cells – IOPscience*, <https://iopscience.iop.org/article/10.1088/2053-1591/ab8c0d>, accessed 2022-09-04.
- 30 S. P. Ong, S. Cholia, A. Jain, M. Brafman, D. Gunter, G. Ceder and K. A. Persson, The Materials Application Programming Interface (API): A Simple, Flexible and Efficient API for Materials Data Based on REpresentational State Transfer (REST) Principles, *Comput. Mater. Sci.*, 2015, **97**, 209–215, DOI: [10.1016/j.commatsci.2014.10.037](https://doi.org/10.1016/j.commatsci.2014.10.037).
- 31 S. P. Ong, W. D. Richards, A. Jain, G. Hautier, M. Kocher, S. Cholia, D. Gunter, V. L. Chevrier, K. A. Persson and G. Ceder, Python Materials Genomics (Pymatgen): A Robust, Open-Source Python Library for Materials Analysis, *Comput. Mater. Sci.*, 2013, **68**, 314–319, DOI: [10.1016/j.commatsci.2012.10.028](https://doi.org/10.1016/j.commatsci.2012.10.028).
- 32 P. Hohenberg and W. Kohn, Inhomogeneous Electron Gas, *Phys. Rev.*, 1964, **136**(3B), B864–B871, DOI: [10.1103/PhysRev.136.B864](https://doi.org/10.1103/PhysRev.136.B864).
- 33 G. Kresse and J. Furthmüller, Efficiency of Ab-Initio Total Energy Calculations for Metals and Semiconductors Using a Plane-Wave Basis Set, *Comput. Mater. Sci.*, 1996, **6**(1), 15–50, DOI: [10.1016/0927-0256\(96\)00008-0](https://doi.org/10.1016/0927-0256(96)00008-0).
- 34 G. Kresse and D. Joubert, From Ultrasoft Pseudopotentials to the Projector Augmented-Wave Method, *Phys. Rev. B: Condens. Matter Mater. Phys.*, 1999, **59**(3), 1758–1775, DOI: [10.1103/PhysRevB.59.1758](https://doi.org/10.1103/PhysRevB.59.1758).
- 35 P. E. Blöchl, Projector Augmented-Wave Method, *Phys. Rev. B: Condens. Matter Mater. Phys.*, 1994, **50**(24), 17953–17979, DOI: [10.1103/PhysRevB.50.17953](https://doi.org/10.1103/PhysRevB.50.17953).
- 36 J. P. Perdew, K. Burke and M. Ernzerhof, Generalized Gradient Approximation Made Simple, *Phys. Rev. Lett.*, 1996, **77**(18), 3865–3868, DOI: [10.1103/PhysRevLett.77.3865](https://doi.org/10.1103/PhysRevLett.77.3865).
- 37 R. Kormath Madam Raghupathy, T. D. Kühne, C. Felser and H. Mirhosseini, Rational Design of Transparent P-Type Conducting Non-Oxide Materials from High-Throughput Calculations, *J. Mater. Chem. C*, 2018, **6**(3), 541–549, DOI: [10.1039/C7TC05311H](https://doi.org/10.1039/C7TC05311H).
- 38 H. J. Monkhorst and J. D. Pack, Special Points for Brillouin-Zone Integrations, *Phys. Rev. B: Solid State*, 1976, **13**(12), 5188–5192, DOI: [10.1103/PhysRevB.13.5188](https://doi.org/10.1103/PhysRevB.13.5188).
- 39 J. Heyd, G. E. Scuseria and M. Ernzerhof, Hybrid Functionals Based on a Screened Coulomb Potential, *J. Chem. Phys.*, 2003, **118**(18), 8207–8215, DOI: [10.1063/1.1564060](https://doi.org/10.1063/1.1564060).
- 40 G. K. H. Madsen, J. Carrete and M. J. Verstraete, BoltzTraP2, a Program for Interpolating Band Structures and Calculating Semi-Classical Transport Coefficients, *Comput. Phys. Commun.*, 2018, **231**, 140–145, DOI: [10.1016/j.cpc.2018.05.010](https://doi.org/10.1016/j.cpc.2018.05.010).
- 41 C. J. Stanton and J. W. Wilkins, Nonequilibrium Current Fluctuations in Semiconductors: A Boltzmann-Equation – Green-Function Approach, *Phys. Rev. B: Condens. Matter Mater. Phys.*, 1987, **35**(18), 9722–9734, DOI: [10.1103/PhysRevB.35.9722](https://doi.org/10.1103/PhysRevB.35.9722).
- 42 V. Wang, N. Xu, J.-C. Liu, G. Tang and W.-T. Geng, VASPKIT: A User-Friendly Interface Facilitating High-Throughput Computing and Analysis Using VASP Code, *Comput. Phys. Commun.*, 2021, **267**, 108033, DOI: [10.1016/j.cpc.2021.108033](https://doi.org/10.1016/j.cpc.2021.108033).
- 43 J. Schmidt, L. Chen, S. Botti and M. A. L. Marques, Predicting the Stability of Ternary Intermetallics with Density Functional Theory and Machine Learning, *J. Chem. Phys.*, 2018, **148**(24), 241728, DOI: [10.1063/1.5020223](https://doi.org/10.1063/1.5020223).
- 44 S. P. Ong, L. Wang, B. Kang and G. Ceder, Li–Fe–P–O2 Phase Diagram from First Principles Calculations, *Chem. Mater.*, 2008, **20**(5), 1798–1807, DOI: [10.1021/cm702327g](https://doi.org/10.1021/cm702327g).
- 45 L. A. Burton, F. Ricci, W. Chen, G.-M. Rignanese and G. Hautier, High-Throughput Identification of Electrides from All Known Inorganic Materials, *Chem. Mater.*, 2018, **30**(21), 7521–7526, DOI: [10.1021/acs.chemmater.8b02526](https://doi.org/10.1021/acs.chemmater.8b02526).
- 46 M. Diaz, L. Wang, D. Li, X. Zhao, B. Conrad, A. Soeriyadi, A. Gerger, A. Lochtefeld, C. Ebert, R. Opila, I. Perez-Wurfl and A. Barnett, Tandem GaAsP/SiGe on Si Solar Cells, *Sol. Energy Mater. Sol. Cells*, 2015, **143**, 113–119, DOI: [10.1016/j.solmat.2015.06.033](https://doi.org/10.1016/j.solmat.2015.06.033).
- 47 J. M. Olson, S. R. Kurtz, A. E. Kibbler and P. Faine, A 27.3% Efficient Ga0.5In0.5P/GaAs Tandem Solar Cell, *Appl. Phys. Lett.*, 1990, **56**(7), 623–625, DOI: [10.1063/1.102717](https://doi.org/10.1063/1.102717).
- 48 W. Setyawan and S. Curtarolo, High-Throughput Electronic Band Structure Calculations: Challenges and Tools, *Comput. Mater. Sci.*, 2010, **49**(2), 299–312, DOI: [10.1016/j.commatsci.2010.05.010](https://doi.org/10.1016/j.commatsci.2010.05.010).
- 49 H. Ding, S. S. Dwaraknath, L. Garten, P. Ndione, D. Ginley and K. A. Persson, Computational Approach for Epitaxial

- Polymorph Stabilization through Substrate Selection, *ACS Appl. Mater. Interfaces*, 2016, **8**(20), 13086–13093, DOI: [10.1021/acsami.6b01630](https://doi.org/10.1021/acsami.6b01630).
- 50 A. Zur and T. C. McGill, Lattice Match: An Application to Heteroepitaxy, *J. Appl. Phys.*, 1984, **55**(2), 378–386, DOI: [10.1063/1.333084](https://doi.org/10.1063/1.333084).
- 51 S. Rühle, The Detailed Balance Limit of Perovskite/Silicon and Perovskite/CdTe Tandem Solar Cells, *Phys. Status Solidi A*, 2017, **214**(5), 1600955, DOI: [10.1002/pssa.201600955](https://doi.org/10.1002/pssa.201600955).
- 52 M. H. Futscher and B. Ehrler, Efficiency Limit of Perovskite/Si Tandem Solar Cells, *ACS Energy Lett.*, 2016, **1**(4), 863–868, DOI: [10.1021/acsenergylett.6b00405](https://doi.org/10.1021/acsenergylett.6b00405).
- 53 I. Almansouri, A. Ho-Baillie, S. P. Bremner and M. A. Green, Supercharging Silicon Solar Cell Performance by Means of Multijunction Concept, *IEEE J. Photovoltaics*, 2015, **5**(3), 968–976, DOI: [10.1109/JPHOTOV.2015.2395140](https://doi.org/10.1109/JPHOTOV.2015.2395140).
- 54 M. K. Y. Chan and G. Ceder, Efficient Band Gap Prediction for Solids, *Phys. Rev. Lett.*, 2010, **105**(19), 196403, DOI: [10.1103/PhysRevLett.105.196403](https://doi.org/10.1103/PhysRevLett.105.196403).
- 55 J. Heyd and G. E. Scuseria, Efficient Hybrid Density Functional Calculations in Solids: Assessment of the Heyd–Scuseria–Ernzerhof Screened Coulomb Hybrid Functional, *J. Chem. Phys.*, 2004, **121**(3), 1187–1192, DOI: [10.1063/1.1760074](https://doi.org/10.1063/1.1760074).
- 56 J. W. Precker and M. A. da Silva, Experimental Estimation of the Band Gap in Silicon and Germanium from the Temperature–Voltage Curve of Diode Thermometers, *Am. J. Physiol.*, 2002, **70**(11), 1150–1153, DOI: [10.1119/1.1512658](https://doi.org/10.1119/1.1512658).
- 57 T. K. Bera, J.-H. Song, A. J. Freeman, J. I. Jang, J. B. Ketterson and M. G. Kanatzidis, Soluble Direct-Band-Gap Semiconductors LiAsS_2 and NaAsS_2 : Large Electronic Structure Effects from Weak As \cdots S Interactions and Strong Nonlinear Optical Response, *Angew. Chem., Int. Ed.*, 2008, **47**(41), 7828–7832, DOI: [10.1002/anie.200801392](https://doi.org/10.1002/anie.200801392).
- 58 W. L. Kehl, R. G. Hay and D. Wahl, The Structure of Tetragonal Tungsten Trioxide, *J. Appl. Phys.*, 1952, **23**(2), 212–215, DOI: [10.1063/1.1702176](https://doi.org/10.1063/1.1702176).
- 59 O. M. Strok, I. D. Oleksyuk, O. F. Zmyi, I. A. Ivashchenko and L. D. Gulay, The Quasi-Ternary System Cu_2Se - Ga_2Se_3 - GeSe_2 , *J. Phase Equilib. Diffus.*, 2013, **34**(2), 94–103, DOI: [10.1007/s11669-013-0188-3](https://doi.org/10.1007/s11669-013-0188-3).
- 60 F. Gao, S. Yamazoe, T. Maeda and T. Wada, Structural Study of Cu-Deficient $\text{Cu}_2(1-x)\text{ZnSnSe}_4$ Solar Cell Materials by X-Ray Diffraction and X-Ray Absorption Fine Structure, *Jpn. J. Appl. Phys.*, 2012, **51**(10S), 10NC28, DOI: [10.1143/JJAP.51.10NC28](https://doi.org/10.1143/JJAP.51.10NC28).
- 61 L. Shi, J. Hu, Y. Qin, Y. Duan, L. Wu, X. Yang and G. Tang, First-Principles Study of Structural, Elastic and Lattice Dynamical Properties of Chalcopyrite BeSiV_2 and MgSiV_2 ($V=\text{P, As, Sb}$), *J. Alloys Compd.*, 2014, **611**, 210–218, DOI: [10.1016/j.jallcom.2014.05.031](https://doi.org/10.1016/j.jallcom.2014.05.031).
- 62 F. A. Weber and T. Schleid, Über Oxidtelluride ($\text{M}_2\text{O}_2\text{Te}$) der leichten Lanthanide ($M = \text{La-Nd, Sm-Ho}$) im A-Typ mitanti-Th Cr_2Si_2 -Struktur, *Z. Anorg. Allg. Chem.*, 1999, **625**(11), 1833–1838, DOI: [10.1002/\(SICI\)1521-3749\(199911\)625:11<1833::AID-ZAAC1833>3.0.CO;2-8](https://doi.org/10.1002/(SICI)1521-3749(199911)625:11<1833::AID-ZAAC1833>3.0.CO;2-8).
- 63 A. Lafond, O. Leynaud, G. Andre, F. Bouree and A. Meerschaut, Magnetic Properties of $\text{Ln}_2\text{Ti}_2\text{S}_2\text{O}_5$ Compounds and Magnetic Structure of $\text{Tb}_2\text{Ti}_2\text{S}_2\text{O}_5$, *J. Alloys Compd.*, 2002, **9**, 185–193.
- 64 G. Cordier, A. Gudat, R. Kniep and A. Rabenau, LiCaN und Li_4SrN_2 , Abkömmlinge Der Fluorit- bzw. Lithiumnitrid-Struktur, *Angew. Chem.*, 1989, **101**(12), 1689–1695, DOI: [10.1002/ange.19891011209](https://doi.org/10.1002/ange.19891011209).
- 65 K. Tolborg, J. Klarbring, A. M. Ganose and A. Walsh, Free Energy Predictions for Crystal Stability and Synthesisability, *ChemRxiv*, 2022, DOI: [10.26434/chemrxiv-2022-vw0dg](https://doi.org/10.26434/chemrxiv-2022-vw0dg), preprint.
- 66 G. Liang, S. Li, Y. Li, L. Wei and X. Zhao, Role of Lone-Pair Electrons in Determining the Thermal Transport Behavior of LiAsS_2 : First-Principles Investigation, *CrystEngComm*, 2021, **23**(23), 4109–4115, DOI: [10.1039/D1CE00120E](https://doi.org/10.1039/D1CE00120E).
- 67 J. A. Brehm, S. M. Young, F. Zheng and A. M. Rappe, First-Principles Calculation of the Bulk Photovoltaic Effect in the Polar Compounds LiAsS_2 , LiAsSe_2 , and NaAsSe_2 , *J. Chem. Phys.*, 2014, **141**(20), 204704, DOI: [10.1063/1.4901433](https://doi.org/10.1063/1.4901433).
- 68 Y. Li and J. Z. Zhang, Hydrogen Generation from Photoelectrochemical Water Splitting Based on Nanomaterials, *Laser Photonics Rev.*, 2009, **4**(4), 517–528, DOI: [10.1002/lpor.200910025](https://doi.org/10.1002/lpor.200910025).
- 69 W. J. Lee, Y. K. Fang, J.-J. Ho, W. T. Hsieh, S. F. Ting, D. Huang and F. C. Ho, Effects of Surface Porosity on Tungsten Trioxide(WO_3) Films' Electrochromic Performance, *J. Electron. Mater.*, 2000, **29**(2), 183–187, DOI: [10.1007/s11664-000-0139-8](https://doi.org/10.1007/s11664-000-0139-8).
- 70 P. P. González-Borrero, F. Sato, A. N. Medina, M. L. Baesso, A. C. Bento, G. Baldissera, C. Persson, G. A. Niklasson, C. G. Granqvist and A. Ferreira da Silva, Optical Band-Gap Determination of Nanostructured WO_3 Film, *Appl. Phys. Lett.*, 2010, **96**(6), 061909, DOI: [10.1063/1.3313945](https://doi.org/10.1063/1.3313945).
- 71 H. Hassani, B. Partoens, E. Bousquet and P. Ghosez, First-Principles Study of Lattice Dynamical Properties of the Room-Temperature P_{2-1}/N and Ground-State P_{2-1}/C Phases of W_3 , *Phys. Rev. B*, 2022, **105**(1), 014107, DOI: [10.1103/PhysRevB.105.014107](https://doi.org/10.1103/PhysRevB.105.014107).
- 72 G. Brunin, F. Ricci, V.-A. Ha, G.-M. Rignanese and G. Hautier, Transparent Conducting Materials Discovery Using High-Throughput Computing, *npj Comput. Mater.*, 2019, **5**(1), 63, DOI: [10.1038/s41524-019-0200-5](https://doi.org/10.1038/s41524-019-0200-5).
- 73 H. Peng, A. Zakutayev, S. Lany, T. R. Paudel, M. d'Avezac, P. F. Ndione, J. D. Perkins, D. S. Ginley, A. R. Nagaraja, N. H. Perry, T. O. Mason and A. Zunger, Li-Doped Cr_2MnO_4 : A New p-Type Transparent Conducting Oxide by Computational Materials Design, *Adv. Funct. Mater.*, 2013, **23**(42), 5267–5276, DOI: [10.1002/adfm.201300807](https://doi.org/10.1002/adfm.201300807).
- 74 G. K. H. Madsen and D. J. Singh, BoltzTraP. A Code for Calculating Band-Structure Dependent Quantities, *Comput. Phys. Commun.*, 2006, **175**(1), 67–71, DOI: [10.1016/j.cpc.2006.03.007](https://doi.org/10.1016/j.cpc.2006.03.007).
- 75 G. Hautier, A. Miglio, D. Waroquiers, G.-M. Rignanese and X. Gonze, How Does Chemistry Influence Electron Effective Mass in Oxides? A High-Throughput Computational

- Analysis, *Chem. Mater.*, 2014, **26**(19), 5447–5458, DOI: [10.1021/cm404079a](https://doi.org/10.1021/cm404079a).
- 76 A. Luque and S. Hegedus, *Handbook of Photovoltaic Science and Engineering*, John Wiley & Sons, 2011.
- 77 J. Gong and S. Krishnan, Mathematical Modeling of Dye-Sensitized Solar Cells, in *Dye-Sensitized Solar Cells*, Elsevier, 2019, pp. 51–81, DOI: [10.1016/B978-0-12-814541-8.00002-1](https://doi.org/10.1016/B978-0-12-814541-8.00002-1).
- 78 V. Fthenakis, Sustainability of Photovoltaics: The Case for Thin-Film Solar Cells, *Renewable Sustainable Energy Rev.*, 2009, **13**(9), 2746–2750, DOI: [10.1016/j.rser.2009.05.001](https://doi.org/10.1016/j.rser.2009.05.001).
- 79 R. Del Sole and R. Girlanda, Optical properties of semiconductors within the independent-quasiparticle approximation, *Phys. Rev. B: Condens. Matter Mater. Phys.*, 1993, **48**, 11789, <https://journals.aps.org/prb/abstract/10.1103/PhysRevB.48.11789>.
- 80 Z. Liu, S. E. Sofia, H. S. Laine, M. Woodhouse, S. Wieghold, I. Marius Peters and T. Buonassisi, Revisiting Thin Silicon for Photovoltaics: A Technoeconomic Perspective, *Energy Environ. Sci.*, 2020, **13**(1), 12–23, DOI: [10.1039/C9EE02452B](https://doi.org/10.1039/C9EE02452B).
- 81 V. Fthenakis, Sustainability of Photovoltaics: The Case for Thin-Film Solar Cells, *Renewable Sustainable Energy Rev.*, 2009, **13**(9), 2746–2750.
- 82 K. Branker, M. J. M. Pathak and J. M. Pearce, A Review of Solar Photovoltaic Levelized Cost of Electricity, *Renewable Sustainable Energy Rev.*, 2011, **15**(9), 4470–4482, DOI: [10.1016/j.rser.2011.07.104](https://doi.org/10.1016/j.rser.2011.07.104).
- 83 S. Chen, X. G. Gong, A. Walsh and S.-H. Wei, Crystal and Electronic Band Structure of Cu₂ZnSnX₄ (X=S and Se) Photovoltaic Absorbers: First-Principles Insights, *Appl. Phys. Lett.*, 2009, **94**(4), 041903, DOI: [10.1063/1.3074499](https://doi.org/10.1063/1.3074499).
- 84 J. Li, D. Wang, X. Li, Y. Zeng and Y. Zhang, Cation Substitution in Earth-Abundant Kesterite Photovoltaic Materials, *Adv. Sci.*, 2018, **5**(4), 1700744, DOI: [10.1002/advs.201700744](https://doi.org/10.1002/advs.201700744).
- 85 W. Wang, M. T. Winkler, O. Gunawan, T. Gokmen, T. K. Todorov, Y. Zhu and D. B. Mitzi, Device Characteristics of CZTSSe Thin-Film Solar Cells with 12.6% Efficiency, *Adv. Energy Mater.*, 2014, **4**(7), 1301465, DOI: [10.1002/aenm.201301465](https://doi.org/10.1002/aenm.201301465).
- 86 *Doping and alloying of kesterites – IOPscience*, <https://iopscience.iop.org/article/10.1088/2515-7655/ab23bc>, accessed 2022-06-12.
- 87 R. Nitsche, D. F. Sargent and P. Wild, Crystal Growth of Quaternary 122464 Chalcogenides by Iodine Vapor Transport, *J. Cryst. Growth*, 1967, **1**(1), 52–53, DOI: [10.1016/0022-0248\(67\)90009-7](https://doi.org/10.1016/0022-0248(67)90009-7).
- 88 G. Gurieva, S. Levchenko, V. C. Kravtsov, A. Nateprov, E. Irran, Y.-S. Huang, E. Arushanov and S. Schorr, X-Ray Diffraction Investigation on Cu₂ZnSnSe₄ Single and Polycrystalline Crystals, *Z. Kristallogr. - Cryst. Mater.*, 2015, **230**(8), 507–511, DOI: [10.1515/zkri-2014-1825](https://doi.org/10.1515/zkri-2014-1825).
- 89 Y. Hinuma, T. Hatakeyama, Y. Kumagai, L. A. Burton, H. Sato, Y. Muraba, S. Iimura, H. Hiramatsu, I. Tanaka, H. Hosono and F. Oba, Discovery of Earth-Abundant Nitride Semiconductors by Computational Screening and High-Pressure Synthesis, *Nat. Commun.*, 2016, **7**(1), 11962, DOI: [10.1038/ncomms11962](https://doi.org/10.1038/ncomms11962).
- 90 X. Lin, J. Kavalakkatt, M. Ch. Lux-Steiner and A. Ennaoui, Inkjet-Printed Cu₂ZnSn(S, Se)₄ Solar Cells, *Adv. Sci.*, 2015, **2**(6), 1500028, DOI: [10.1002/advs.201500028](https://doi.org/10.1002/advs.201500028).
- 91 J. J. Scragg, P. J. Dale and L. M. Peter, Towards Sustainable Materials for Solar Energy Conversion: Preparation and Photoelectrochemical Characterization of Cu₂ZnSnS₄, *Electrochem. Commun.*, 2008, **10**(4), 639–642, DOI: [10.1016/j.elecom.2008.02.008](https://doi.org/10.1016/j.elecom.2008.02.008).
- 92 A. Crovetto, A. Cazzaniga, R. B. Ettliger, J. Schou and O. Hansen, Optical Properties and Surface Characterization of Pulsed Laser-Deposited Cu₂ZnSnS₄ by Spectroscopic Ellipsometry, *Thin Solid Films*, 2015, **582**, 203–207, DOI: [10.1016/j.tsf.2014.11.075](https://doi.org/10.1016/j.tsf.2014.11.075).
- 93 Q. Guo, G. M. Ford, W.-C. Yang, B. C. Walker, E. A. Stach, H. W. Hillhouse and R. Agrawal, Fabrication of 7.2% Efficient CZTSSe Solar Cells Using CZTS Nanocrystals, *J. Am. Chem. Soc.*, 2010, **132**(49), 17384–17386, DOI: [10.1021/ja108427b](https://doi.org/10.1021/ja108427b).
- 94 L. A. Burton, Y. Kumagai, A. Walsh and F. Oba, DFT Investigation into the Underperformance of Sulfide Materials in Photovoltaic Applications, *J. Mater. Chem. A*, 2017, **5**(19), 9132–9140, DOI: [10.1039/C7TA00673J](https://doi.org/10.1039/C7TA00673J).